

# Highly Conductive Carbon Nanotube-Graphene Hybrid Yarn

Javad Foroughi,\* Geoffrey M. Spinks, Dennis Antiohos, Azadehsadat Mirabedini, Sanjeev Gambhir, Gordon G. Wallace, Shaban R. Ghorbani, Germanas Peleckis, Mikhail E. Kozlov, Marcio D. Lima, and Ray H. Baughman

An efficient procedure for the fabrication of highly conductive carbon nanotube/graphene hybrid yarns has been developed. To start, arrays of vertically aligned multi-walled carbon nanotubes (MWNT) are converted into indefinitely long MWNT sheets by drawing. Graphene flakes are then deposited onto the MWNT sheets by electrospinning to form a composite structure that is transformed into yarn filaments by twisting. The process is scalable for yarn fabrication on an industrial scale. Prepared materials are characterized by electron microscopy, electrical, mechanical, and electrochemical measurements. It is found that the electrical conductivity of the composite MWNT-graphene yarns is over 900 S/cm. This value is 400% and 1250% higher than electrical conductivity of pristine MWNT yarns or graphene paper, respectively. The increase in conductivity is associated with the increase of the density of states near the Fermi level by a factor of 100 and a decrease in the hopping distance by an order of magnitude induced by graphene flakes. It is found also that the MWNT-graphene yarn has a strong electrochemical response with specific capacitance in excess of 111 Fg<sup>-1</sup>. This value is 425% higher than capacitance of pristine MWNT yarn. Such substantial improvements of key properties of the hybrid material can be associated with the synergy of MWNT and graphene layers in the yarn structure. Prepared hybrid yarns can benefit such applications as high-performance supercapacitors, batteries, high current capable cables, and artificial muscles.

the assemblies can be extended by incorporating particles of various functional materials in their structures with the aid of “bi-scrolling” technology.<sup>[5]</sup> Because of the combination of high surface area with good electrical and mechanical properties nanostructured, macroscopic fibers can be beneficial for diverse applications. The functionally enhanced yarns can be used in such areas as advanced catalytic converters, battery electrodes and superconducting cables. Electrochemical and thermal stimulation of pristine and enhanced yarns resulted in the discovery of a family of torsional and tensile actuators capable of providing unexpectedly high power and energy densities.<sup>[6,7]</sup> The infiltration of yarns and their precursors with an elastomeric polymer binder led to the development of conductive and highly stretchable composites<sup>[5,8]</sup> that can be employed for high-stroke strain sensors, touch-sensitive skin for robots or stretchable electronic devices.

In this paper we explore a new type of conductive composite prepared by the electro-spinning of a chemically converted

graphene (CCG) within and on the surface of MWNT yarns. The procedure developed for the fabrication is substantially different from conventional composite fabrication processes in which polymer and carbon nanotube fillers are mixed and then shaped to form a fiber or film. In our case, the CCG dispersion was incorporated into the pre-formed MWNT forest using electrospinning. The composite yarn exhibited improved mechanical, electrical and electrochemical properties as compared with the pristine MWNT material and graphene sheets.

## 1. Introduction

The preparation of carbon nanotube (CNT) assemblies by fibre spinning processes enables their production in practically viable quantities.<sup>[1–4]</sup> The range of properties available from

Dr. J. Foroughi, Prof. G. M. Spinks, Dr. D. Antiohos, A. Mirabedini, Dr. S. Gambhir, Prof. G. G. Wallace  
ARC Centre of Excellence for Electromaterials Science  
University of Wollongong  
Wollongong, NSW, 2519, Australia  
E-mail: Foroughi@uow.edu.au

Prof. S. R. Ghorbani  
Department of Physics  
Ferdowsi University of Mashhad  
Mashhad, Iran

Dr. G. Peleckis  
Institute for Superconducting and Electronic Materials  
University of Wollongong  
Wollongong, NSW 2519, Australia

Dr. M. E. Kozlov, Dr. M. D. Lima, Prof. R. H. Baughman  
Alan G MacDiarmid NanoTech Institute  
University of Texas at Dallas  
Richardson, TX 75083, USA



DOI: 10.1002/adfm.201401412

## 2. Results and Discussion

### 2.1. Preparation of Hybrid Yarns

Hybrid CNT/graphene yarn has been continuously produced using CNT web as a host material and graphene dispersions as guest. As can be seen from **Figure 1** the CNT web could be continuously drawn from the spinnable CNT forest to create the electrospinning collector. The drawn CNT web was connected to the DC electric motor. The resultant graphene coated CNT web could be continuously twisted to develop the hybrid CNT/

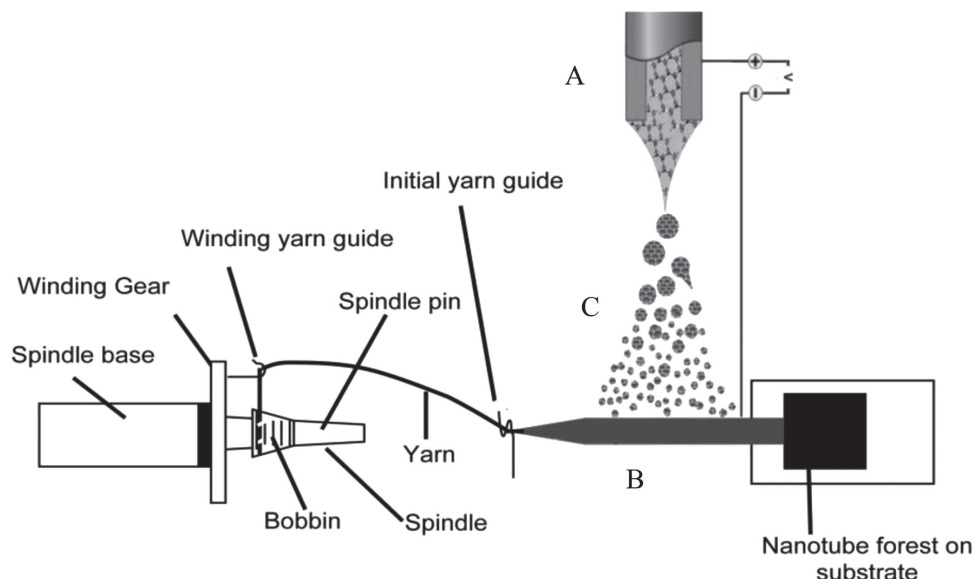


**Figure 1.** Schematic diagram of continuously produced hybrid CNT/graphene yarn. (A) Electrospinning setup used for graphene deposition; (B) MWNT sheet drawn from spinable forest and employed as graphene collector; (C) graphene dispersion (electrospray).

graphene yarn. The direction of twist could be in clockwise (right or S twist) or anticlockwise (left or Z twist). In our case, twist insertion into the hybrid CNT/graphene yarn was carried out in S (right) direction. The current method has an ability to scaled up and semicontinuously or continuously produce the hybrid CNT/graphene yarn. The amount of graphene incorporated into the hybrid yarn could be varied using different feeding rate of graphene and/or duration of electrospay. Thermogravimetric analysis (TGA) has been carried out to estimate the amount of graphene in the yarn. The TGA results confirmed that as-prepared hybrid CNT-graphene yarn has approximately 5% weight graphene (see supporting information).

## 2.2. Morphology of CNT-Graphene Yarn

SEM micrographs of the pristine CNT forest and yarns are shown in **Figure 2(a-b)**. As can be seen from the surface morphology, the nanotubes were uniformly oriented with respect to the yarn axis. The surface morphology of the as-prepared CNT/graphene yarns (**Figure 2d-e**) was completely different from the pristine CNT yarn. The graphene sheets were clearly presented on the surface of CNT/graphene yarn in **Figure 2(d-e)** and their presence altered the twist-induced yarn structure giving a furrowed surface texture. The SEM image of the cross-section of hybrid CNT/graphene yarn (**Figure 2c and f**) shows that the as-prepared CNT/graphene yarn has a porous structure.

## 2.3. Mechanical Properties of CNT/Graphene Yarn

The mechanical properties of hybrid carbon nanotube/graphene yarn show that the ultimate tensile strength, elastic modulus and elongation at break were  $140 \pm 10$  MPa,  $2.58 \pm 0.3$  GPa and  $6 \pm 2\%$ , respectively. While the tensile strength of hybrid CNT/graphene yarn is similar to pristine CNT yarn

(150 to 500 MPa), the elongation at break of the CNT/graphene yarn was 100% higher than pristine CNT yarn ( $3 \pm 2\%$ ).<sup>[2]</sup> The elastic modulus of as-prepared yarn was quite low compared to pristine CNT yarn due to porous nature of the CNT/graphene yarn (see **Figure 2 C** and supporting information).

## 2.4. Electrochemical Properties of CNT/Graphene Yarn

The CNT/graphene yarn electrochemical response is presented as a free standing yarn, wrapped throughout a fine and flexible Pt mesh to insure good contact between the yarn and the Pt mesh current collector. The reasons for doing so is to try and mimic its use for real world applications where costly and bulky current collectors need to be avoided so as to reduce size and increase flexibility. Potential multi-functional devices that can utilise yarns include thermoacoustic loudspeakers,<sup>[9]</sup> weavable electrodes for flexible current collectors,<sup>[10]</sup> electrical shielding,<sup>[11]</sup> and supercapacitors.<sup>[12]</sup> The advantage of our material is that there is a strong electrochemical response for the free standing CNT/graphene yarn as can be seen by **Figure 3**. In the Nyquist plot of **Figure 3a** (inset) at high frequencies, a small depressed semi-circle is apparent which is approximately  $5.35 \text{ Ohm.cm}^2$  indicating fast ion diffusion.<sup>[13]</sup> The series resistance (intercept of Z Real with the x-axis) is low at  $2.16 \text{ Ohm.cm}^2$  signifying good connection of the active materials to each other and the current collector. The imaginary part of the impedance rapidly rises at low frequencies indicating capacitive type behaviour.<sup>[14]</sup> The cyclic voltammograms (CVs) of **Figure 3b** were obtained from the two electrode cell at varying scan rates. It can be seen that at high scan rates of  $2000 \text{ mV/s}$ , the CV curve is square and very symmetrical indicating a fast charge/discharge process at the electrode/electrolyte interface. As the scan rate is decreased, the CV diagram reflects larger capacitive behaviour where full charging/discharging of the material can occur, leading to good electrochemical reversibility and an increase in

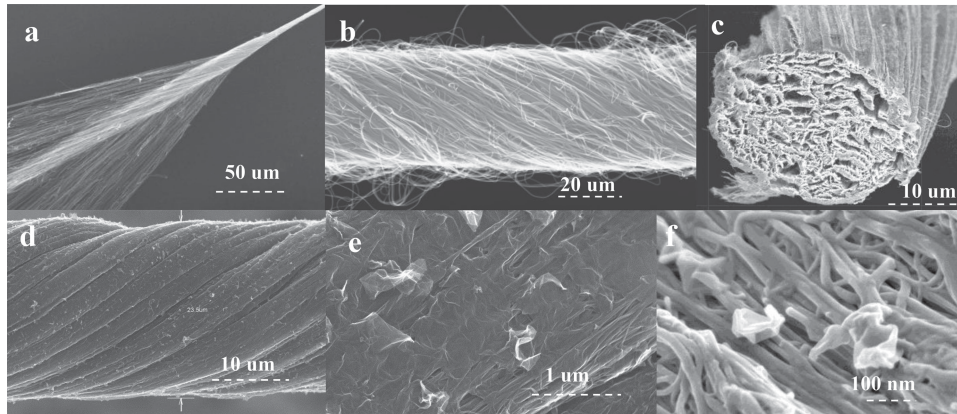


**Figure 2.** SEM images of (a) CNT forest during twist insertion to form pristine yarns; (b) pristine CNT yarn; hybrid carbon nanotube-graphene yarn: cross-section (c) at low and (f) high magnification; hybrid yarn surface (d) at low and (e) high magnification.

the utilisation of the electroactive surface area.<sup>[15]</sup> The specific capacitance per electrode at 2 mV/s and 2000 mV/s was calculated using the following equation<sup>[16]</sup>

$$C_{sp}(\text{mass}) = 2 \frac{I}{m} \frac{dv}{dt} \quad (1)$$

$$C_{sp}(\text{area}) = 2 \frac{I}{A} \frac{dv}{dt} \quad (2)$$

where  $I$  is the average current  $(I_{\text{anodic}} - I_{\text{cathodic}})/2$ ,  $dV/dt$  is the potential sweep rate (V/s),  $m$  is the mass of nanocomposite yarn at each electrode, and  $A$  is the area of the yarn (yarn area is assumed to be cylindrical). A factor of 2 is incorporated due to the series capacitance formed in a two-electrode system. (It must be noted that both the specific capacitance as a function of mass and area has been evaluated as this is important in commercial standards and applications).<sup>[17]</sup> The values obtained at 2 mV/s were 212 mF/cm<sup>2</sup> and 111 F/g, respectively. While the values obtained at faster scan rates of 2000 mV/s was 3.1 mF/cm<sup>2</sup> and 3.5 F/g, respectively. As a comparison, Foroughi *et al.* have reported in previous work that polypyrrole-MWNT yarns achieved 60 Fg<sup>-1</sup> in 0.10M lithium bis(trifluoromethanesulfonyl)imide/propylene carbonate,<sup>[18]</sup>

while Mirfakhrai *et al.* reported pristine CNT yarns that achieved a specific capacitance of 26 Fg<sup>-1</sup> in 0.5 M tetrabutylammonium tetrafluoroborate/acetonitrile.<sup>[19]</sup> Lee *et al.* reported a volumetric capacitance 179 Fcm<sup>-3</sup> (1 M H<sub>2</sub>SO<sub>4</sub>) for PEDOT/MWNT yarns that were wrapped around a Pt wire for electrochemical testing.<sup>[20]</sup>

## 2.5. Electrical and Transport Properties of CNT/Graphene Yarn

The electrical conductivity of the CNT and CNT/Graphene yarns have been measured under laboratory humidity and temperature conditions by an in-house linear four-point probe cell. The average electrical conductivity of CNT and CNT/Graphene yarns were  $220 \pm 20$  and  $900 \pm 50$  S/cm, respectively. The electrical conductivity of graphene paper obtained from chemically converted graphene was reported to be 72 S/cm.<sup>[21]</sup> It was found that the electrical conductivity of MWNT/graphene yarn was 400% and 1250% higher than obtained from the pristine MWNT yarn and graphene paper, respectively. The higher electrical conductivity of as-prepared CNT/graphene yarn suggests a lower contact resistivity between nanotube bundles due to the presence of the graphene sheets.

The temperature dependence of conductance  $G(T)$  and conductivity  $\sigma(T)$  of CNT/graphene and pristine CNT yarns are shown in Figure 4. As can be seen from Figure 4 (inset), the

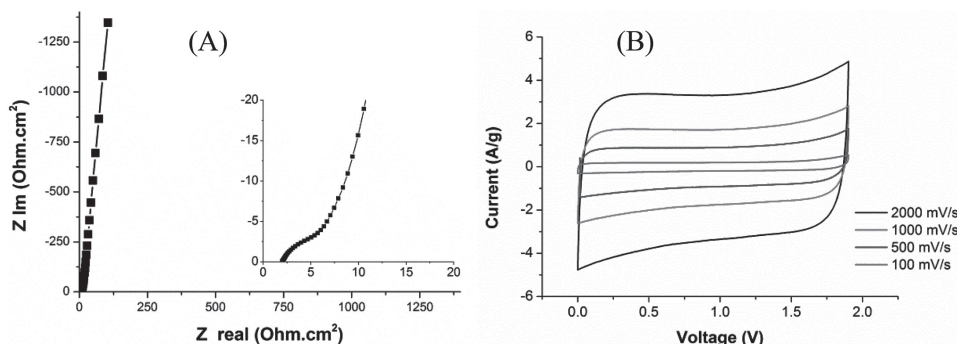


**Figure 3.** MWNT/graphene yarn tested in a two electrode configuration. (a) Nyquist plot, (b) CV at varying scan rates. Electrolyte is 1 M LiClO<sub>4</sub>/acetonitrile. Mass of each yarn is 0.15 mg with a 50 μm diameter and 5 cm length.

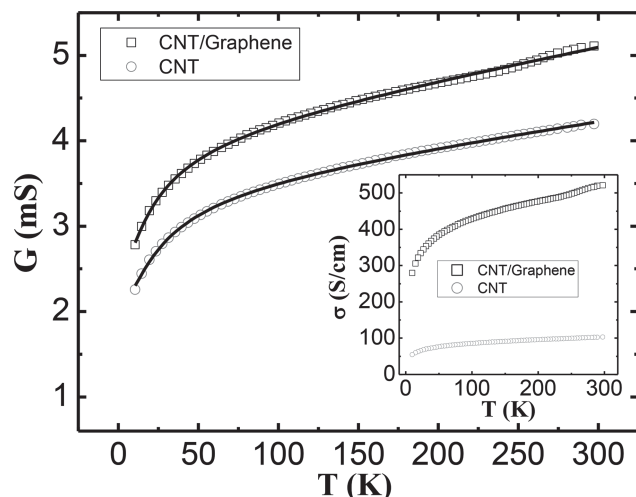


**Figure 4.** The temperature dependence of conductance  $G(T)$  of the CNT yarn and CNT/graphene yarn. The solid curves show the two shell model fitting to experimental data. Inset: Conductivity as a function of temperature for both samples.

conductivity as function of temperature for the CNT/graphene yarn has higher conductivity than the pristine CNT yarn over the whole range of temperatures measured.

This figure clearly indicates the decrease in conductivity with a decrease in temperature. Such behavior was observed in both multi-walled carbon nanotubes (MWNTs) and single-walled carbon nanotubes (SWNTs), where the temperature dependence was fitted to a power-law function. For MWNTs, this behavior was explained in terms of Luttinger liquid (LL) model.<sup>[26]</sup> Other mechanisms like thermally activated transport ( $\ln G(T) \propto -1/T$ ), weak localization ( $G(T) \propto \ln T$ )<sup>[22]</sup> and variable-range hopping (VRH),<sup>[23]</sup> that suppress the conductance at lower temperatures, and a model involving conduction in the two outer shell (two shell model),<sup>[24]</sup> were also considered. However, in the present system, we have found that VRH and two shell models gives a good fit to our data. In disordered systems, the low temperature transport is governed by VRH between the localized states. Mott<sup>[25]</sup> predicted the key relation for the temperature dependence of conductivity for non-interacting carriers and for a constant density of states near the Fermi energy. At low temperatures, it was concluded by Mott<sup>[25]</sup> that the electrons seek accessible energy states by hopping distances beyond the localization length, leading to the variable-range hopping mechanism. The temperature dependent on the conductivity of conducting polymers is commonly explained by the three-dimensional variable range hopping (3D-VRH) model<sup>[25]</sup>

$$\sigma(T) = \frac{\sigma_0}{\sqrt{T}} \exp\left(\frac{T_0}{T^{1+d}}\right) \quad (3)$$

where  $\sigma_0$  is the high temperature limit of dc conductivity,  $d$  is the dimensionality of the conduction process of the system, and  $T_0 = (\lambda\alpha^3 / \lambda\alpha^3 k_B - k_B N(E_F))^{1/4}$  is related to thermally activated hopping among localized states.  $N(E_F)$  is the density of localized states at  $E_F$ ,  $\lambda$  is a dimensionless constant,  $\alpha^{-1}$  represents the spatial extension of the wave function  $\exp(-\alpha R)$  associated

with the localized states. It was found<sup>[26]</sup> that the value of  $\sigma_0$  and  $N(E_F)$  are given by:

$$\alpha = 22.5\sigma_0 T_0^2 \text{ cm}^{-1} \quad (4)$$

and

$$N(E_F) = 2.12 \times 10^9 \sigma_0^3 T_0^2 \text{ cm}^{-3} \cdot eV^{-1} \quad (5)$$

The average hopping distance  $R_{\text{hop}}$  between two sites and the activation energy  $W_{\text{hop}}$  are<sup>[25]</sup>

$$R_{\text{hop}} = \left(\frac{9}{8\pi\alpha k_B T N(E_F)}\right)^{1/4} \quad (6)$$

$$W_{\text{hop}} = \left(\frac{3}{4\pi R_{\text{hop}}^3 N(E_F)}\right) \quad (7)$$

Evaluation of  $\ln(\sigma T^{1/2})$  vs.  $T^{-1/(1+d)}$  with  $d = 1, 2$  and  $3$  showed good fits to the experimental data only for  $d = 3$ . As can be seen in **Figure 5**, the conductivity of the CNT yarn and CNT/graphene have a similar behaviour as a function of temperature and both fit well to the 3D-VRH model. In both cases a crossover temperature of  $\sim 80$  K was observed that separated two regions in the temperature dependence of conductivity. The conductivity is evaluated from the best fitted straight lines at temperature intervals higher than the crossover temperature of 80 K and lower than 80 K as presented in **Figure 5**. The best fitted values of  $\sigma_0$  and  $T_0$  are shown in **Tables 1** and **2** for both samples in both regions.

Using Equations (4)–(7), various Mott's parameters like  $N(E_F)$ ,  $\alpha$ ,  $R_{\text{hop}}$  ( $T = 300$  K), and  $W_{\text{hop}}$  ( $T = 300$  K), are calculated

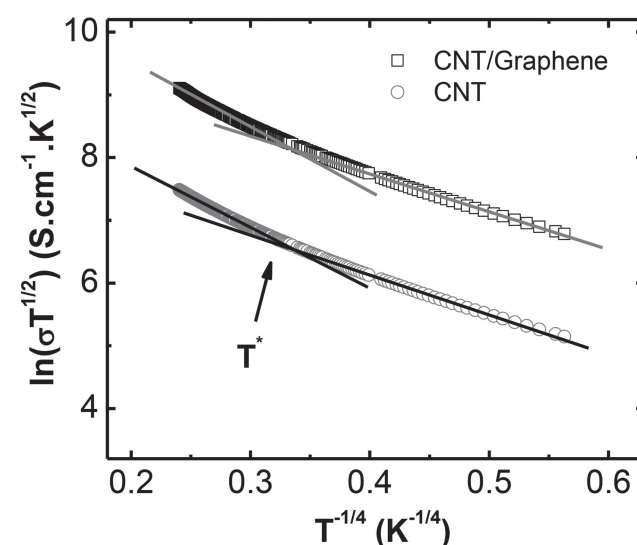


**Figure 5.** Temperature dependence of dc conductivity of the CNT yarn and CNT/graphene yarn. The arrow shows the crossover temperature  $T^*$  between two regions. Solid lines are fits to Equation (3).

**Table 1.** Conductivity analysis based on VRH model for the samples.

Sample	$T_0$ [K <sup>1/4</sup> ]	$\sigma_0$ [10 <sup>3</sup> S/cm]	$\alpha$ [nm <sup>-1</sup> ]	$N(E_F)$ [10 <sup>22</sup> eV <sup>-1</sup> .cm <sup>-3</sup> ]	$R_{\text{hop}}$ (T = 300 K) [nm]	$W_{\text{hop}}$ [meV]
T > 80 K						
CNT	9.74	18.3	0.129	4.06	1.28	2.83
CNT-Graphene	9.85	93.2	0.657	537.54	0.25	2.84
T < 80 K						
CNT	6.26	5.7	0.0323	0.0987	4.57	2.56
CNT-Graphene	6.18	27.6	0.154	11.073	0.95	2.55

and presented in Tables 1 and 2. The calculated value of density of states near the Fermi level obtained using Mott's VRH relations comes out to be  $4 \times 10^{22}$  and  $537 \times 10^{22}$  eV<sup>-1</sup> cm<sup>-3</sup> at temperature higher than  $T^* = 80$  K and at temperature lower than 80 K they are  $1 \times 10^{21}$  and  $110 \times 10^{21}$  eV<sup>-1</sup> cm<sup>-3</sup> for the CNT and CNT/graphene yarn, respectively. These results show that the density of states near the Fermi level of the CNT/graphene is larger than that for the CNT yarn by an order of 2. For one-layer carbon nanotube and MWNTs film, the density of states at Fermi level was reported to be  $\sim 10^{21}$  eV<sup>-1</sup> cm<sup>-3</sup> and  $7.5 \times 10^{19}$  eV<sup>-1</sup> cm<sup>-3</sup>,<sup>[26,27]</sup> respectively. This result indicates that charge carriers are more delocalized by the presence of graphene. Therefore, the value of  $N(E_F)$  is higher in the CNT/graphene compare to the reported  $N(E_F)$  value by an order of 3–4 at room temperature. The obtained average hopping distance by using the Equation (6) at room temperature for the CNT/graphene yarn shown in Table 1 is about 0.25 nm while for the CNT yarn it increases to about 1.28 nm, in agreement with previous report for MWNTs film,<sup>[27]</sup> above the crossover temperature  $T^* = 80$  K and it increases about 4 times at temperatures below  $T^* = 80$  K. Therefore, graphene decreases the hopping distance by an order of 1. The estimated activation energies for hopping as shown in Table 1 is 2.8 above  $T^*$  and 2.5 meV below  $T^*$  for both samples. This values agree well with the average hopping distance changes. The spatial extension of the wave function,  $\alpha^{-1}$ , associated with the localized states for the CNT/graphene yarn is larger than that in the CNT yarn by a factor about 6 (see Table 1). The obtained result of  $N(E_F)$ ,  $\alpha$ , and  $R_{\text{hop}}$  (T = 300 K) confirm that graphene improved the conductivity in CNT yarn as can be seen in Figure 4.

Based on the electrical conductivity relationship with temperature fitting the one dimensional VRH (1D-VRH), it has already been shown that 1D-VRH conduction is the dominant electron transfer mechanism in disordered MWNT.<sup>[28]</sup> CNT yarns, regardless of being pristine or composite, are predominantly made of a group of MWNTs that are aligned and packed in an ordered structure as result of van der Waals interactions.

**Table 2.** Conductance analysis based on two shell model for the samples.

Sample	$G_{10}$ [mS]	A [μS/K]	$G_{20}$ [mS]	$T_b$ [K]
CNT	2.14	2.67	1.39	24.8
CNT-Graphene	2.55	3.56	1.59	20.6

One can then regard these elongated back to back strands of MWNTs as disordered MWNTs. Therefore, the observed behavior can be explained and appears realistic. In addition, at the ends of every piece of MWNT in the yarn the electrons have the likelihood of switching direction and moving to other nearby strands of MWNTs. This fact explains the three dimensional characteristic of the fitting model.

From the electrical conductance measurements, it was found that individual multiwall carbon nanotubes (MWNTs) mostly show a metallic behavior.<sup>[29,30]</sup> It was also inferred that conduction in MWNTs takes place mostly in the outer shell,<sup>[31]</sup> but recent results reveal a substantial contribution from conduction in the second shell after carriers tunnel from the outer shell.<sup>[32]</sup> Therefore, two shell model was suggested to analyze the electronic transport of MWNTs by Skákalová et al.<sup>[24]</sup> They proposed that thermally assisted transfer of electrons from the outer shell to the inner shell and the activated or fluctuation-assisted tunneling<sup>[33]</sup> current through the inner shell are two main mechanisms for flowing of current through MWNTs. Based on the two shell model the conductance are given by:

$$G(T) = G_1 + G_{20} \exp\left(-\frac{T_b}{T + T_s}\right) \quad (8)$$

where  $G_1 = G_{10} + AT$  incorporates a term increasing linearly with temperature  $T$  due to the conductance of the outer shell between the voltage electrodes.  $T_b$  is the order of magnitude of typical barrier energies indicated by the value of  $k_B T_b$  and the ratio  $T_s/T_b$  shows the decrease of conductivity at low temperatures. The solid curves in Figure 3 shows the results of fitting the Equation (8) to the experiment conductance  $G(T)$  data of the CNT yarn, CNT/graphene. It can be seen in Figure 3, the two shell model (Equation (8)) gave a very good description of the temperature dependence of conductance for both samples within the temperature range studied. Therefore, the results of two shell model are in good agreement with a three dimensional characteristic of the MWNT yarns conductivity and it supported the 3D conductivity behavior that inferred from the three-dimensional variable range hopping (3D-VRH) model.

The best fitted values of two shell model parameters are shown in Table 2 for the samples. The fitted value of the activation energy  $k_B T$  was 2.14 and 1.78 meV ( $T_b = 24.8$  and 20.6 K) for the CNT yarn and the CNT/graphene yarn, respectively. For both samples, the parameter  $T_s$  was zero, i.e., a simple activated form was adequate to describe the nonlinear temperature dependence.

### 3. Conclusions

We developed a novel approach to produce high performance bicomponent multi walled carbon nanotube/graphene yarn. Electrospinning has been used to introduce graphene sheets into the carbon nanotube yarn using chemically converted graphene dispersion as the spinning solution and drawn CNT forest as collector. This novel all-carbon process has been developed for the fabrication of highly conductive carbon nanotube/graphene hybrid yarns. The mechanical strength and Young's modulus of as-prepared yarn were 140 MPa and 2.58 GPa, respectively. The electrical conductivity of composite MWNT-graphene yarns (over 900 S/cm) was significantly higher than those of pristine MWNT yarns prepared for comparison. This value was 400% and 1250% higher than obtained from pristine MWNT yarns or graphene paper, respectively. The conductivity shows 3D behaviour and it does not correspond to a one or two dimensional variable range hopping model. It was found from 3D-VRH model that the graphene increased the density of states near the Fermi level by an order of 2 and also decreased the hopping distance by an order of 1 result charge carriers are more delocalized and significant increased electrical conductivity of the CNT/graphene yarn.

It was found that the free standing MWNT/graphene yarn has a strong electrochemical response in which the specific capacitance of composite yarns was found to exceed  $111 \text{ Fg}^{-1}$ . This value was 425% higher than obtained from pristine MWNT yarn. Such substantial improvements of key properties of composite yarns can be associated with synergy of MWNT and graphene layers in yarn structure. The developed process is scalable for yarn fabrication on an industrial scale. Prepared hybrid yarns can benefit such applications as high-performance supercapacitors, batteries, high current capable cables and artificial muscles.

## 4. Experimental Section

### 4.1. Materials

#### 4.1.1. Synthesis of Carbon Nanotubes

Drawable carbon multiwalled nanotube forests for producing CNT/graphene yarns were grown by chemical vapor deposition (CVD) on silicon wafers coated by iron catalyst using acetylene ( $\text{C}_2\text{H}_2$ ) gas as the carbon precursor. Transmission and scanning electron microscope (SEM) images of the  $\sim 400 \mu\text{m}$  high forests indicate that the MWNTs have an outer diameter of  $\sim 12 \text{ nm}$ , contain  $\sim 9$  walls, and form large bundles as described previously.<sup>[2,34]</sup>

#### 4.1.2. Preparation of Chemically Converted Graphene Dispersions

Preparation of graphene oxide (GO) and chemically converted graphene (CCG) dispersions have been described previously.<sup>[21,35]</sup> Graphene oxide (62.5 g) was diluted with deionised water (2 L) and sonicated for 80 min. Then, hydrazine monohydrate (64–65%) (400  $\mu\text{l}$ ) and ammonia (4 ml) were added and the solution was heated at 90 °C for 1 h. A further aliquot of hydrazine (3 ml) was added to the solution and the mixture was heated and kept at 90 °C for 2 h under constant stirring. After cooling to the room temperature, the solution was acidified with  $\text{H}_2\text{SO}_4$  (aq. 30%), then the agglomerated graphene

powder was washed until the waste water was at a neutral pH. The agglomerated graphene powder was filtered and dried in vacuum at 50 °C for 2 days. To form a stable suspension, dried CCG (300 mg) was added to dimethylformamide (DMF) (150 ml, moisture content  $\leq 350 \text{ ppm}$  by Karl-Fischer). Triethylamine (50  $\mu\text{l}$ ) was added and the solution was extensively sonicated with continuous cooling under a dry nitrogen purge. Further DMF (300 ml) and triethylamine (500  $\mu\text{l}$ ) were then added and the suspension was further sonicated under nitrogen. The dispersion was centrifuged to separate any agglomerated graphene sheets and the resulting supernatant (0.5  $\text{mg ml}^{-1}$ ) was stable for several months without any agglomeration. Stability of dispersion in organic solvents has significantly improved by controlling the chemically modified edges with charged functional groups on CCG. The dominating repulsive interactions leading to stable dispersions were achieved by reducing the lateral size of the sheet by excessive ultrasonication. As a result of this, the dispersion is stable for several months without any aggregation. Procedure of preparing the dispersion and its application for preparing tough composites has been reported by us.<sup>[36,37]</sup> The zeta potential of the dispersion is below  $-30 \text{ eV}$  over a period of several months. Non-contact atomic force microscopy (AFM) shows sheets displaying a uniform trapezoidal morphology for organic dispersion and is in good agreement with the solution particle sizing, the size of the CCG sheet was approximately 300 – 400 nanometres with an average thickness of approximately 0.97 nm. A detailed study of preparing the stable dispersion in anhydrous organic solvents with varying degree of reduction of graphene oxide and its characterisation is under publication by us.

#### 4.1.3. Preparation of Hybrid CNT/Graphene Yarn

Figure 1 shows a schematic diagram of the electrospinning setup used to prepare the carbon nanotube/graphene yarn. The needle was connected to the high-voltage supply, which can generate positive DC voltages up to 35 kV. The distance between the tip of the needle and the collector was 15 cm. Positive voltages (15 kV) over applied to the needle containing the graphene dispersion in DMF. The solution flow rates were controlled with a syringe pump ranging from 0.5 to 1 mL/h. A CNT web drawn from the CVD deposited nanotubes was used as collector. The drawn CNT web also was connected to the DC electric motor to provide the twist into the graphene coated CNT yarn. All electrospinning experiments were carried out at room temperature (24 °C) and at relative humidity below 30%.

### 4.2. Characterisation

Scanning electron microscopy (SEM) images were collected with a field-emission SEM instrument (JEOL JSM-7500FA). The mechanical properties of the yarn were measured using a tensile testing instrument (Shimadzu EZ-L) with a 10 N load cell. Samples were prepared by attaching yarn to paper frames (10 mm) using superglue. Samples were mounted on the sample holder and paper was cut. Three samples were tested and strain rate was set to 10 mm/min. The TGA characteristics of pristine CNT yarn, graphene film and hybrid CNT-graphene yarn were studied from room temperature to 1000 °C (TA Instrument Q500 thermal gravimetric analyzer) at a heating rate of 10 °C/min in an Argon purge. Electrical conductivity of fibres was measured under laboratory humidity and temperature conditions by an in-house linear four-point probe cell with 230  $\mu\text{m}$  probe spacing using a galvanostat (Princeton Applied Research 363) to apply current between outer probes and a digital multimeter (Agilent 34401A) to measure resulting voltage between the two inner probes. Each yarn was wrapped in a fine Pt mesh to provide electrical connection. A two electrode configuration ("simulated supercapacitor") was built by placing each individual yarn/Pt mesh inside a sealed glass testtube, each spaced 4 mm apart with 1 M  $\text{LiClO}_4$ /acetonitrile as the electrolyte for all electrochemical measurements. The yarn length was 5 cm and the diameter was approximately 50  $\mu\text{m}$ .

Electrochemical impedance spectroscopy (EIS) measurements were performed at room temperature using the two electrode set up where the frequency range spanned 100 kHz to 0.01 Hz with an AC amplitude of 10 mV (rms) at open circuit potential using a Gamry EIS 3000 system. Cyclic voltammetry (CV) studies of the MWNT/graphene yarn were performed at room temperature again using the two electrode set up with electrochemical analysis system (EDAQ Australia) with EChem V 2 software (ADI Instruments Pty. Ltd). The potential window studied was between 0 V and 2.1 V. The electrolyte was 1 M LiClO<sub>4</sub> in acetonitrile. Electrical transport of the carbon nanotubes and CNT-graphene yarns was characterized by standard four probe technique (Quantum Design PPMS). All measured yarns were placed onto MgO substrate and four Au wires were attached using silver paste.

## Supporting Information

Supporting Information is available from the Wiley Online Library or from the author.

## Acknowledgements

This work has been supported by the Australian Research Council under Discovery Early Career Researcher award (DE12010517), through the Centres of Excellence (ACES) scheme for financial support and Australian National Fabrication Facility (ANFF). The authors thank Ali Jirani for assistance with Figures 1.

Received: May 1, 2014  
Published online:

- [1] M. E. Kozlov, R. C. Capps, W. M. Sampson, V. H. Ebron, J. P. Ferraris, R. H. Baughman, *Adv. Mater.* **2005**, *17*(5) 614–617
- [2] M. Zhang, K. R. Atkinson, R. H. Baughman, *Science* **2004**, *306*(5700) 1358–1361.
- [3] W. Zhou, J. Vavro, C. Guthy, K. I. Winey, J. E. Fischer, L. M. Ericson, S. Ramesh, R. Saini, V. A. Davis, C. Kittrell, M. Pasquali, R. H. Hauge, R. E. Smalley, *J. Appl. Phys.* **2004**, *95*(2) 649–655.
- [4] H. W. Zhu, C. L. Xu, D. H. Wu, B. Q. Wei, R. Vajtai, P. M. Ajayan, *Science* **2002**, *296*(5569) 884–886.
- [5] M. D. Lima, S. L. Fang, X. Lepro, C. Lewis, R. Ovalle-Robles, J. Carretero-Gonzalez, E. Castillo-Martinez, M. E. Kozlov, J. Y. Oh, N. Rawat, C. S. Haines, M. H. Haque, V. Aare, S. Stoughton, A. A. Zakhidov, R. H. Baughman, *Science* **331**(6013) 51–55.
- [6] J. Foroughi, G. M. Spinks, G. G. Wallace, J. Oh, M. E. Kozlov, S. Fang, T. Mirfakhrai, J. D. W. Madden, M. K. Shin, S. J. Kim, R. H. Baughman, *Science* **2011**, *334*(6055) 494–497.
- [7] M. D. Lima, N. Li, M. Jung de Andrade, S. Fang, J. Oh, G. M. Spinks, M. E. Kozlov, C. S. Haines, D. Suh, J. Foroughi, S. J. Kim, Y. Chen, T. Ware, M. K. Shin, L. D. Machado, A. F. Fonseca, J. D. W. Madden, W. E. Voit, D. S. Galvão, R. H. Baughman, *Science* **2012**, *338*(6109) 928–932.
- [8] M. K. Shin, J. Oh, M. Lima, M. E. Kozlov, S. J. Kim, R. H. Baughman, *Adv. Mater.* **2010**, *22*(24) 2663–2667.
- [9] Y. Wei, X. Lin, K. Jiang, P. Liu, Q. Li, S. Fan, *Nano Letters* **2013**, *13*(10) 4795–4801.
- [10] C.-F. Sun, H. Zhu, E. B. Baker Iii, M. Okada, J. Wan, A. Gemes, Y. Inoue, L. Hu, Y. Wang, *Nano Energy* **2013**, *2*(5) 987–994.
- [11] A. Bedelogleu, *J. Tex. Inst.* **2013**, *104*(11) 1247–1257.
- [12] K. Jia, X. Zhuang, B. Cheng, S. Shi, Z. Shi, B. Zhang, *J. Mater. Sci.: Mater. Electron.* **2013**, *24*(12) 4769–4773.
- [13] H. Liu, P. He, Z. Li, Y. Liu, J. Li, *Electrochim. Acta* **2006**, *51*(10) 1925–1931.
- [14] S. H. Aboutalebi, A. T. Chidembo, M. Salari, K. Konstantinov, D. Wexler, H. K. Liu, S. X. Dou, *Energy Environ. Sci.* **2011**, *4*(5) 1855–1865.
- [15] Z. H. Dong, Y. L. Wei, W. Shi, G. A. Zhang, *Mater. Chem. Phys.* **2011**, *131*(1–2) 529–534.
- [16] A. K. Mishra, S. Ramaprabhu, *J. Phys. Chem. C* **2011**, *115*(29) 14006–14013.
- [17] Z. Niu, W. Zhou, J. Chen, G. Feng, H. Li, W. Ma, J. Li, H. Dong, Y. Ren, D. Zhao, S. Xie, *Energy Environ. Sci.* **2011**, *4*(4) 1440–1446.
- [18] J. Foroughi, G. M. Spinks, S. R. Ghorbani, M. E. Kozlov, F. Safaei, G. Peleckis, G. G. Wallace, R. H. Baughman, *Nanoscale* **2012**, *4*(3) 940–945.
- [19] T. Mirfakhrai, J. Oh, M. Kozlov, E. C. W. Fok, M. Zhang, S. Fang, R. H. Baughman, J. D. W. Madden, *Smart Mater. Struct.* **2007**, *16*(2) S243.
- [20] J. A. Lee, M. K. Shin, S. H. Kim, H. U. Cho, G. M. Spinks, G. G. Wallace, M. D. Lima, X. Lepro, M. E. Kozlov, R. H. Baughman, S. J. Kim, *Nat. Commun.* **2013**, *4*.
- [21] D. Li, M. B. Muller, S. Gilje, R. B. Kaner, G. G. Wallace, *Nat. Nanotechnol.* **2008**, *3*(2) 101–105.
- [22] L. Langer, V. Bayot, E. Grivei, J. P. Issi, J. P. Heremans, C. H. Olk, L. Stockman, C. Van Haesendonck, Y. Bruynseraede, *Phys. Rev. Lett.* **1996**, *76*(3) 479–482.
- [23] Y.-H. Lee, D.-H. Kim, K. Hoon, B.-K. Ju, *J. Appl. Phys.* **2000**, *88*(7) 4181–4185.
- [24] V. Skákalová, A. B. Kaiser, Y. S. Woo, S. Roth, *Phys. Rev. B* **2006**, *74*(8) 085403.
- [25] N. F. Mott, E. A. Davis, *Electronic Processes in Non-Crystalline Materials* Clarendon Press, Oxford, **2012**.
- [26] M. Aggarwal, S. Khan, M. Husain, T. C. Ming, M. Y. Tsai, T. P. Perng, Z. H. Khan, *Eur. Phys. J. B Condens. Matter Complex Syst.* **2007**, *60*(3) 319–324.
- [27] V. I. Tsebro, O. E. Omel'yanovskii, E. F. Kukovitskii, N. A. Sainov, N. A. Kiselev, D. N. Zakharov, *J. Exptl. Theor. Phys.* **1998**, *86*(6) 1216–1220.
- [28] D. P. Wang, D. E. Feldman, B. R. Perkins, A. J. Yin, G. H. Wang, J. M. Xu, A. Zaslavsky, *Solid State Comm.* **2007**, *142*(5) 287–291.
- [29] T. W. Ebbesen, H. J. Lezec, H. Hiura, J. W. Bennett, H. F. Ghaemi, T. Thio, *Nature* **1996**, *382*(6586) 54–56.
- [30] S. N. Song, X. K. Wang, R. P. H. Chang, J. B. Ketterson, *Phys. Rev. Lett.* **1994**, *72*(5) 697–700.
- [31] A. Bachtold, C. Strunk, J.-P. Salvetat, J.-M. Bonard, L. Forro, T. Nussbaumer, C. Schonenberger, *Nature* **1999**, *397*(6721) 673–675.
- [32] B. Bourlon, C. Miko, L. Forró, D. C. Glatli, A. Bachtold, *Phys. Rev. Lett.* **2004**, *93*(17) 176806.
- [33] P. Sheng, *Phys. Rev. B* **1980**, *21*(6) 2180–2195.
- [34] K. R. Atkinson, S. C. Hawkins, C. Huynh, C. Skourtis, J. Dai, M. Zhang, S. Fang, A. A. Zakhidov, S. B. Lee, A. E. Aliev, C. D. Williams, R. H. Baughman, *Phys. B: Condens. Matter* **2007**, *394*(2) 339–343.
- [35] W. S. Hummers, R. E. Offeman, *J. Am. Chem. Soc.* **1958**, *80*(6) 1339–1339.
- [36] S. Sayyar, E. Murray, B. C. Thompson, S. Gambhir, D. L. Officer, G. G. Wallace, *Carbon* **2013**, *52*(0) 296–304.
- [37] M. K. Shin, B. Lee, S. H. Kim, J. A. Lee, G. M. Spinks, S. Gambhir, G. G. Wallace, M. E. Kozlov, R. H. Baughman, S. J. Kim, *Nat. Commun.* **2012**, *3*, 650.